CrossMark

J. Fluid Mech. (2016), *vol.* 804, *pp.* 370–386. © Cambridge University Press 2016
doi:10.1017/jfm.2016.528

Bounds for convection between rough boundaries

David Goluskin[1,†] **and Charles R. Doering**[1,2]

[1]Department of Mathematics and Center for the Study of Complex Systems, University of Michigan, Ann Arbor, MI 48109, USA

[2]Department of Physics, University of Michigan, Ann Arbor, MI 48109, USA

(Received 28 April 2016; revised 29 June 2016; accepted 5 August 2016; first published online 9 September 2016)

We consider Rayleigh–Bénard convection in a layer of fluid between rough no-slip boundaries where the top and bottom boundary heights are functions of the horizontal coordinates with square-integrable gradients. We use the background method to derive an upper bound on the mean heat flux across the layer for all admissible boundary geometries. This flux, normalized by the temperature difference between the boundaries, can grow with the Rayleigh number (Ra) no faster than $O(Ra^{1/2})$ as $Ra \to \infty$. Our analysis yields a family of similar bounds, depending on how various estimates are tuned, but every version depends explicitly on the boundary geometry. In one version the coefficient of the $O(Ra^{1/2})$ leading term is $0.242 + 2.925\|\nabla h\|^2$, where $\|\nabla h\|^2$ is the mean squared magnitude of the boundary height gradients. Application to a particular geometry is illustrated for sinusoidal boundaries.

Key words: Bénard convection, variational methods

1. Introduction

Average transport properties of turbulent fluid flows, such as mixing efficiencies or fluxes of momentum and heat, are often of more interest than details of any particular flow realization. One way to estimate mean quantities is to numerically integrate the equations of motion over a long time and then average. Of course, the broad range of scales present in turbulence makes such direct numerical simulations challenging. An alternate approach is to derive mathematical bounds on mean quantities. Although such bounds might not be as close to 'true' values as the results of simulations, they have certain advantages. First, bounds are proven directly on infinite-time averages whereas simulations may be subject to long transients. Second, bounds apply to all possible initial conditions whereas an attracting state reached in one simulation does not preclude the existence of other attracting states. Finally, bounds may be derived as functions of the relevant parameters and, as in the present work, for a variety of geometries within some class. In contrast, simulations must be repeated for every new parameter value or geometry, and they often cannot access the extreme parameter regimes relevant for many astrophysical, geophysical and engineering applications.

† Email address for correspondence: goluskin@umich.edu

https://doi.org/10.1017/jfm.2016.528 Published online by Cambridge University Press

Mathematical methods for bounding turbulent transport properties have largely focused on the simple geometry of a fluid layer confined by smooth planar walls. For channels and shear flows, upper bounds on wall drag coefficients have been derived rigorously from the incompressible Navier–Stokes equations (Busse 1969; Howard 1972; Constantin & Doering 1994, 1995; Kerswell 1997; Nicodemus, Grossmann & Holthaus 1998; Hoffmann & Vitanov 1999; Kerswell 2002; Plasting & Kerswell 2003; Seis 2015). For buoyancy-driven thermal convection between planar boundaries, the authors and others have proven lower bounds on mean temperature (Lu, Doering & Busse 2004; Whitehead & Doering 2011*a*, 2012; Goluskin 2015*a*,*b*) and upper bounds on heat transport (Howard 1963; Constantin & Doering 1996; Kerswell 1997, 2001; Otero *et al.* 2002; Plasting & Ierley 2005; Wittenberg 2010; Otto & Seis 2011; Whitehead & Doering 2011*b*, 2012; Wang & Whitehead 2013; Wen *et al.* 2013; Whitehead & Wittenberg 2014; Choffrut, Nobili & Otto 2016).

Domain geometries in applications are often more complicated than a plane layer, however, and physical boundaries are never perfectly smooth. Such boundary variations can significantly affect mean quantities of interest, so closing the gap between theory and experiment requires the establishment of bounds that are valid for geometrically complicated or rough boundaries. Here, we present a way to do so using the background method, a variational method used to prove many of the above-cited bounds in simple geometries. Complicated geometries have been studied previously by Wang (1997), who bounded dissipation in certain shear-driven flows, albeit without computing explicit constants. Here, we study thermal convection by a somewhat different approach which produces explicit bounds.

The particular problem that we consider in this paper is Rayleigh–Bénard convection where a layer of fluid heated from below and cooled from above is confined between non-intersecting top and bottom boundaries that are no-slip and perfectly conductive (that is, isothermal). Unlike the canonical configuration of Rayleigh (1916) in which the cooler upper and warmer lower boundaries are perfectly flat planes, we allow the boundary heights to be continuous piecewise differentiable functions of the horizontal coordinates. As previously accomplished for planar boundaries, we derive an upper bound on the net vertical heat flux across the fluid layer as a function of the temperature difference between the boundaries and the relevant material and geometric parameters. Such bounds are typically expressed in terms of the dimensionless Nusselt and Rayleigh numbers, Nu and Ra, where Nu is the factor by which convection amplifies heat transfer beyond diffusive transport and Ra is proportional to the temperature difference across the layer. For finite-Prandtl-number fluids between no-slip planar boundaries, the best upper bound proven to date is $Nu \lesssim 0.027\,Ra^{1/2}$ (Plasting & Kerswell 2003).

In this work we prove an upper bound on heat transport that also scales proportionally to $Ra^{1/2}$, albeit with a prefactor that depends on the details of the boundary geometry. This result is consistent with past experimental and numerical studies of convection between rough boundaries (Du & Tong 1998, 2000; Villermaux 1998; Ciliberto & Laroche 1999; Roche *et al.* 2001; Stringano, Pascazio & Verzicco 2006; Salort *et al.* 2014; Wei *et al.* 2014; Toppaladoddi, Succi & Wettlaufer 2015; Wagner & Shishkina 2015), all of which report that roughness can enhance heat transport, and some of which report that it increases the rate at which Nu grows with Ra. The fastest growth rate reported is $Ra^{1/2}$ in the experiments of Roche *et al.* (2001) where all boundaries were rough, including the sidewalls.

Section 2 defines the mathematical model we study, and § 3 lays out key integral relations and the meanings of various integral quantities, including the Nusselt number. The main result is proven in § 4, and its application to a particular geometry is illustrated for sinusoidal boundaries. Section 5 offers conclusions and open challenges.

https://doi.org/10.1017/jfm.2016.528 Published online by Cambridge University Press

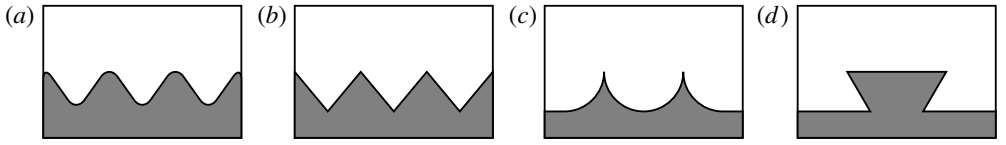


FIGURE 1. Examples of boundaries to which our main result does and does not apply. It applies to boundaries specified by continuous and piecewise differentiable functions whose gradients are (*a*) continuous or (*b*) piecewise continuous, including (*c*) gradients that are unbounded but square-integrable, but not to (*d*) boundaries that are not functions of the horizontal coordinates.

2. Configuration

We employ the Oberbeck–Boussinesq approximation with constant kinematic viscosity ν, thermal diffusivity κ and coefficient of thermal expansion α. We non-dimensionalize such that the length scale d is the difference between the maximum height of the top boundary and the minimum height of the bottom one, the time scale d^2/κ is that of thermal diffusion and the temperature scale Δ is the temperature difference between the top and bottom boundaries. Then, the dimensionless Boussinesq equations governing the velocity $\boldsymbol{u} = (u, v, w)$, temperature T and pressure p are

$$\boldsymbol{u}_t + \boldsymbol{u}\cdot\boldsymbol{\nabla}\boldsymbol{u} = -\boldsymbol{\nabla}p + Pr\,\nabla^2\boldsymbol{u} + Pr\,Ra\,T\hat{\boldsymbol{z}}, \tag{2.1}$$

$$T_t + \boldsymbol{u}\cdot\boldsymbol{\nabla}T = \nabla^2 T, \tag{2.2}$$

$$\boldsymbol{\nabla}\cdot\boldsymbol{u} = 0. \tag{2.3}$$

The Rayleigh and Prandtl numbers are $Ra = (g\alpha d^3\Delta)/\kappa\nu$ and $Pr = \nu/\kappa$, where g is the acceleration of gravity in the $-\hat{\boldsymbol{z}}$ direction. Here, z is the vertical coordinate, while x and y are horizontal. Subscripts of t, x, y or z denote partial derivatives.

The top and bottom boundaries of the domain are specified by $z = h^T(x, y)$ and $z = h^B(x, y)$, continuous functions that can model both small-scale roughness and large-scale features. Our proof relies on the boundaries being continuous piecewise differentiable functions of the horizontal coordinates and on the gradients $\boldsymbol{\nabla}h^T$ and $\boldsymbol{\nabla}h^B$ being square-integrable. Examples of boundary geometries to which our main result does and does not apply are shown in figures 1(*a–c*) and 1(*d*) respectively.

Lengths are non-dimensionalized so that the maximum of $h^T(x, y)$ and the minimum of $h^B(x, y)$ differ by unity. We choose $z = 0$ to coincide with the minimum of $h^B(x, y)$; hence, the vertical domain is

$$0 \leqslant h^B(x, y) \leqslant z \leqslant h^T(x, y) \leqslant 1. \tag{2.4}$$

Figure 2 is a schematic of the set-up we have in mind. The origin of the temperature scale is arbitrary, so for the thermal boundary conditions we can fix

$$T|_{z=h^B(x,y)} = 1, \quad T|_{z=h^T(x,y)} = 0. \tag{2.5a,b}$$

When the boundaries are planar, standard Rayleigh–Bénard convection is recovered with $h^B \equiv 0$ and $h^T \equiv 1$. The horizontal coordinates (x, y) are assumed to lie in a bounded two-dimensional domain Ω whose boundary is piecewise differentiable. In each horizontal direction the flow can be either periodic (with h^B and h^T also periodic)

https://doi.org/10.1017/jfm.2016.528 Published online by Cambridge University Press

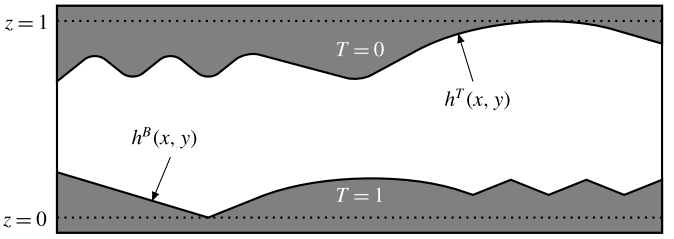


FIGURE 2. Example two-dimensional slice of our non-dimensionalized configuration.

or bounded by perfectly insulating vertical sides. If there are no periodic directions, our three-dimensional domain is a cylinder with (possibly complicated) cross-section Ω and rough end caps defined by h^B and h^T. Consideration of non-vertical sidewalls is left for future work. We impose no-slip ($\boldsymbol{u}=\boldsymbol{0}$) conditions on the top and bottom boundaries. If sidewalls exist, the velocity conditions there can be either no-slip or free-slip. The existence of piecewise smooth solutions to the three-dimensional Boussinesq equations is unproven even in simple geometries, but our results apply to such solutions whenever they exist.

Unless there is no buoyancy ($Ra=0$), the configuration we are considering does not generally admit a static state – that is, a solution to the equations of motion with $\boldsymbol{u}=\boldsymbol{0}$ and $T_t=0$. This is distinct from the case of planar boundaries where the static solution exists for all Ra and is stable when $Ra<1707.7$ (Jeffreys 1928). Indeed, a static state must satisfy $\nabla^2 T=0$ and $\boldsymbol{\nabla} p = Pr\,Ra\,T\hat{\boldsymbol{z}}$. Such a stationary harmonic temperature field generally exists, but the buoyancy force field it induces can only be balanced by the pressure if $Ra\,T\hat{\boldsymbol{z}}$ is a gradient – that is, only if $Ra=0$ or if h^B and h^T are constant so that the static T field depends on z alone.

3. Integral quantities

We wish to bound the dimensionless time-averaged heat flux across the layer, $\mathscr{F}$. For concreteness we define $\mathscr{F}$ as the inward heat flux across the bottom boundary, although it follows from the temperature equation (2.2) that the time-averaged heat flux is the same across any surface within the fluid that spans the domain horizontally. At each point on the bottom boundary, the inward heat flux is equal to the outward temperature gradient, $\hat{\boldsymbol{n}}\cdot\boldsymbol{\nabla}T$. Integrating over the bottom surface and averaging over infinite time gives the definition

$$\mathscr{F} := \lim_{t\to\infty}\frac{1}{t}\int_0^t \mathrm{d}t' \int_{\{z=h^B\}} \mathrm{d}S\,\hat{\boldsymbol{n}}\cdot\boldsymbol{\nabla}T(x,y,z,t'). \tag{3.1}$$

Here, we assume that infinite-time averages exist, but this assumption could be avoided by employing lim sup in place of lim. The main result that we establish in § 4 is an upper bound on $\mathscr{F}$ that scales like $Ra^{1/2}$ at large Ra.

Let angular brackets denote volume integrals and infinite-time averages:

$$\langle f\rangle := \lim_{t\to\infty}\frac{1}{t}\int_0^t \mathrm{d}t' \iint_\Omega \mathrm{d}x\,\mathrm{d}y \int_{h^B(x,y)}^{h^T(x,y)} \mathrm{d}z\, f(x,y,z,t'). \tag{3.2}$$

Our calculations are expressed in terms of volume integrals, as opposed to volume averages, so enlarging the horizontal extent tends to increase $\mathscr{F}$. Integrating

https://doi.org/10.1017/jfm.2016.528 Published online by Cambridge University Press

$\langle T \times (2.2)\rangle$ and $\langle \boldsymbol{u} \cdot (2.1)\rangle$ by parts yields the integral relations

$$\langle |\boldsymbol{\nabla} T|^2 \rangle = \mathscr{F}, \tag{3.3}$$

$$\langle |\boldsymbol{\nabla} \boldsymbol{u}|^2 \rangle = Ra \langle wT \rangle. \tag{3.4}$$

Time derivatives do not appear in these relations because the volume integrals of $|\boldsymbol{u}|$ and $|T|$ are bounded uniformly in time, a fact that follows from the present analysis (cf. Constantin & Doering 1996).

The heat flux $\mathscr{F}$ that we want to bound is related *a priori* to the thermal dissipation $\langle |\boldsymbol{\nabla} T|^2 \rangle$ but not to the viscous dissipation $\langle |\boldsymbol{\nabla} \boldsymbol{u}|^2 \rangle$. With planar boundaries, $\mathscr{F}$ is related also to $\langle |\boldsymbol{\nabla} \boldsymbol{u}|^2 \rangle$ because it is tied to the mean vertical convection $\langle wT \rangle$ by $\mathscr{F} = A + \langle wT \rangle$, where $A = |\Omega|$ is the area of the horizontal cross-section. With non-planar boundaries, on the other hand, a given flux $\mathscr{F}$ can coincide with various values of $\langle wT \rangle$, depending on how the heat transport is distributed horizontally. If a larger fraction of convective transport occurs in regions where the layer is thin, $\langle wT \rangle$ will be smaller, essentially because conduction within the boundaries helps more with upward heat transport.

Implementations of the background method for Rayleigh–Bénard convection with planar boundaries have exploited the fact that $\mathscr{F}$ is related to both $\langle |\boldsymbol{\nabla} T|^2 \rangle$ and $\langle |\boldsymbol{\nabla} \boldsymbol{u}|^2 \rangle$ (e.g. Constantin & Doering 1996; Kerswell 2001). Since non-planar boundaries spoil this feature, our implementation is more similar to lower bounds on mean temperature proven for internally heated convection. Mean temperature in such configurations, like $\mathscr{F}$ here, is related *a priori* to $\langle |\boldsymbol{\nabla} T|^2 \rangle$ but not to $\langle |\boldsymbol{\nabla} \boldsymbol{u}|^2 \rangle$ (Lu *et al.* 2004; Whitehead & Doering 2011*a*, 2012; Goluskin 2015*a*,*b*).

Heat transport in convection is typically quantified by a Nusselt number Nu that is in some sense a ratio of total transport to conductive transport. Defining both transports as volume averages in the flowing fluid has proven useful for revealing parallels between various thermal boundary conditions (Otero *et al.* 2002; Johnston & Doering 2009; Wittenberg 2010; Goluskin 2015*b*). However, it is unclear how to extend this definition to complicated geometries, partly because the convective transport $\langle wT \rangle$ is no longer related *a priori* to the total transport. The natural alternative is to normalize $\mathscr{F}$ by the heat flux in the static state that exists when $Ra = 0$. Defined in this way, Nu is unity in the static state and is suitably insensitive to the domain size. Furthermore, the bound that we prove on $\mathscr{F}$ implies an upper bound on Nu that scales proportionally to $Ra^{1/2}$, as in the case of planar boundaries.

4. Upper bound on heat transport

Rather than bound $\mathscr{F}$ subject to the constraint that $\boldsymbol{u}$ and T solve the Boussinesq equations (2.3)–(2.2), we bound $\mathscr{F}$ subject to relaxed constraints on $\boldsymbol{u}$ and T that are satisfied by all such solutions. In particular, the only constraints we impose are incompressibility, boundary conditions on $\boldsymbol{u}$ and T, three integral relations implied by the Boussinesq equations and the extremum principle $0 \leqslant T \leqslant 1$ holding at large times. The analysis of this section culminates in an explicit bound on $\mathscr{F}$ for general boundaries in § 4.6, followed by its application to sinusoidal boundaries in § 4.7.

4.1. *Background decomposition*

The background method is implemented by decomposing the temperature field as

$$T(x, y, z, t) = \tau(x, y, z) + \theta(x, y, z, t), \tag{4.1}$$

https://doi.org/10.1017/jfm.2016.528 Published online by Cambridge University Press

where τ is the so-called background field. We choose an explicit expression for τ that is continuous and satisfies the same boundary conditions as T, so θ is continuous and satisfies homogeneous boundary conditions.

The first two integral constraints we require are the dissipation balances (3.3) and (3.4). The latter, obtained by integrating $\langle \theta \times (2.2) \rangle$ by parts, is

$$\langle \boldsymbol{\nabla}\tau \cdot \boldsymbol{\nabla}\theta \rangle = -\langle \theta \boldsymbol{u} \cdot \boldsymbol{\nabla}\tau \rangle - \langle |\boldsymbol{\nabla}\theta|^2 \rangle. \tag{4.2}$$

Our only use for these integral constraints is to derive a particular equality for $\mathscr{F}$:

$$\begin{aligned} \mathscr{F} &= \langle |\boldsymbol{\nabla}\tau|^2 \rangle + 2\langle \boldsymbol{\nabla}\tau \cdot \boldsymbol{\nabla}\theta \rangle + \langle |\boldsymbol{\nabla}\theta|^2 \rangle & (4.3)\\ &= \langle |\boldsymbol{\nabla}\tau|^2 \rangle - 2\langle \theta \boldsymbol{u} \cdot \boldsymbol{\nabla}\tau \rangle - \langle |\boldsymbol{\nabla}\theta|^2 \rangle & (4.4)\\ &= \langle |\boldsymbol{\nabla}\tau|^2 \rangle + \left[a\langle \tau w \rangle - \frac{a}{Ra}\langle |\boldsymbol{\nabla}\boldsymbol{u}|^2 \rangle - \langle \theta \boldsymbol{u} \cdot (2\boldsymbol{\nabla}\tau - a\hat{\boldsymbol{z}}) \rangle - \langle |\boldsymbol{\nabla}\theta|^2 \rangle \right], & (4.5) \end{aligned}$$

where $a > 0$ remains to be specified. The first line above is the expansion of (3.3) in terms of τ and θ, the next follows from (4.2) and the third is reached by adding $a[\langle w(\tau + \theta) \rangle - (1/Ra)\langle |\boldsymbol{\nabla}\boldsymbol{u}|^2 \rangle]$, which is zero according to (3.4).

If the boundaries were planar we could choose τ to make the part of (4.5) in brackets non-positive, thereby proving $\mathscr{F} \leqslant \langle |\boldsymbol{\nabla}\tau|^2 \rangle$. However, doing so relies partly on choosing a horizontally uniform τ to make $\langle \tau w \rangle$ vanish, and with rough boundaries this would violate the boundary conditions on τ. Instead, we can prove an upper bound on the bracketed expression that is larger than zero but of the same order in Ra as the $\langle |\boldsymbol{\nabla}\tau|^2 \rangle$ term. We will do this in two pieces, splitting the $\langle |\boldsymbol{\nabla}\boldsymbol{u}|^2 \rangle$ term to obtain

$$\mathscr{F} = \langle |\boldsymbol{\nabla}\tau|^2 \rangle + \mathscr{Q}_1 + \mathscr{Q}_2, \tag{4.6}$$

where

$$\mathscr{Q}_1[\boldsymbol{u}, \theta] := -\left[(1-\gamma)\frac{a}{Ra}\langle |\boldsymbol{\nabla}\boldsymbol{u}|^2 \rangle + \langle \theta \boldsymbol{u} \cdot (2\boldsymbol{\nabla}\tau - a\hat{\boldsymbol{z}}) \rangle + \langle |\boldsymbol{\nabla}\theta|^2 \rangle \right], \tag{4.7}$$

$$\mathscr{Q}_2[\boldsymbol{u}] := a\langle \tau w \rangle - \gamma \frac{a}{Ra}\langle |\boldsymbol{\nabla}\boldsymbol{u}| \rangle^2 \tag{4.8}$$

and $\gamma \in (0, 1)$ will be chosen later.

We will construct a background field τ for which each term in (4.6) is no larger than $O(Ra^{1/2})$. Regarding $\mathscr{Q}_1$ and $\mathscr{Q}_2$ as quadratic functionals of unknown fields θ and $\boldsymbol{u}$, we prove upper bounds that hold for all θ and incompressible $\boldsymbol{u}$ that satisfy the boundary conditions.

4.2. *Choice of background field*

The continuous background field $\tau(x, y, z)$ will be defined piecewise in three regions: top and bottom boundary layers of uniform height δ, and the remaining interior. The boundary layers must be thin enough to not overlap; planar boundaries require $\delta < 1/2$ and non-planar boundaries require yet smaller δ. The τ considered here has affine z-dependence in all three regions, which leads to tractable analysis. A more general ansatz would yield a tighter bound but not necessarily a different scaling from $Ra^{1/2}$.

Figure 3 shows the structure of the background field τ. In the interior region, $\tau = 1/2$ on the $z = 1/2$ plane and $\boldsymbol{\nabla}\tau = (0, 0, a/2)$. This $\boldsymbol{\nabla}\tau$ makes the sign-indefinite term of $\mathscr{Q}_1$ vanish pointwise outside the boundary layers, which helps us to show in § 4.3 that $\mathscr{Q}_1 \lesssim O(Ra^{1/2})$. The definition of τ on the interior dictates values at the

https://doi.org/10.1017/jfm.2016.528 Published online by Cambridge University Press

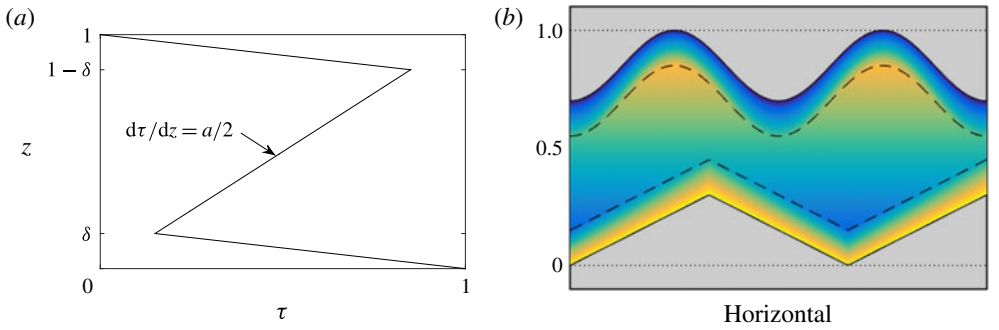


FIGURE 3. (Colour online) Examples of the chosen background field τ with $a = 2$ and boundary layer thickness $\delta = 0.15$. (*a*) A graph of $\tau(z)$ for planar boundaries. (*b*) A two-dimensional slice of $\tau(x, y, z)$ for non-planar boundaries, with τ ranging from 1 (light) on the bottom boundary to 0 (dark) on the top one. The $\tau(x, y, z)$ field is continuous everywhere, but its gradient is not generally continuous across the boundary layer edges (– – –).

edges of the boundary layers that depend on h^T and h^B, and thus on x and y. In each boundary layer we let τ have an affine dependence on z that interpolates between τ at the boundary layer edge and at the domain boundary. Altogether this means

$$\tau(x, y, z) = \begin{cases} \left[\frac{1}{2} + \frac{a}{2}\left(h^T - \frac{1}{2} - \delta\right)\right]\left(\frac{h^T - z}{\delta}\right), & h^T - \delta \leqslant z \leqslant h^T, \\ \frac{1}{2} + \frac{a}{2}\left(z - \frac{1}{2}\right), & h^B + \delta \leqslant z \leqslant h^T - \delta, \\ 1 - \left[\frac{1}{2} + \frac{a}{2}\left(\frac{1}{2} - h^B - \delta\right)\right]\left(\frac{z - h^B}{\delta}\right), & h^B \leqslant z \leqslant h^B + \delta. \end{cases} \tag{4.9}$$

The background field depends only on z in the interior but generally on all three coordinates in the boundary layers. However, τ is not fully defined until δ and a are chosen. In § 4.3 a particular $O(Ra^{-1/2})$ expression for δ is chosen to ensure $\mathscr{Q}_1 \lesssim O(Ra^{1/2})$. The quantity a must be $O(1)$, and the optimal choice is discussed in § 4.6.

4.3. *Upper bound on* $\mathscr{Q}_1$

In this subsection the quadratic functional $\mathscr{Q}_1[\boldsymbol{u}, \theta]$ defined by (4.7) is bounded above by an $O(Ra^{1/2})$ expression. For the upper bound to be independent of $\boldsymbol{u}$ and θ, the sign-indefinite term $\langle \theta \boldsymbol{u} \cdot (2\boldsymbol{\nabla}\tau - a\hat{\boldsymbol{z}})\rangle$ must be estimated using the sign-definite terms $\langle |\boldsymbol{\nabla}\boldsymbol{u}|^2\rangle$ and $\langle |\boldsymbol{\nabla}\theta|^2\rangle$. Expanding the indefinite term gives

$$|\langle \theta \boldsymbol{u} \cdot (2\boldsymbol{\nabla}\tau - a\hat{\boldsymbol{z}})\rangle| \leqslant \langle |2\tau_x u\theta|\rangle + \langle |2\tau_y v\theta|\rangle + \langle |(2\tau_z - a)w\theta|\rangle. \tag{4.10}$$

All three integrands in the right-hand expression vanish outside the boundary layers, so only the integrals over the boundary layers must be estimated. Let us consider the first and third terms. (The second term is handled like the first.)

The derivatives of τ appearing in (4.10) are bounded pointwise in the bottom boundary layer ($h^B \leqslant z \leqslant h^B + \delta$) by

$$|2\tau_z - a| = \frac{1}{\delta}\left|1 + a\left(\frac{1}{2} - h^B\right)\right| \leqslant \frac{a+2}{2\delta}, \tag{4.11}$$

https://doi.org/10.1017/jfm.2016.528 Published online by Cambridge University Press

$$|2\tau_x| = \frac{1}{\delta}\left|1 + a\left(\frac{1}{2} - h^B\right) - a(h^B + \delta - z)\right| |h_x^B| \leqslant \frac{a+2}{2\delta}|h_x^B| \tag{4.12}$$

for all $\delta < 1/2$. The estimates (4.11)–(4.12) and their analogues in the top boundary layer give

$$\langle|(2\tau_z - a)w\theta|\rangle \leqslant \left(\frac{a+2}{2\delta}\right)[\langle|w\theta|\rangle_B + \langle|w\theta|\rangle_T], \tag{4.13}$$

$$\langle|2\tau_x u\theta|\rangle \leqslant \left(\frac{a+2}{2\delta}\right)[\langle|h_x^B u\theta|\rangle_B + \langle|h_x^T u\theta|\rangle_T], \tag{4.14}$$

where $\langle\cdot\rangle_B$ and $\langle\cdot\rangle_T$ are defined like (3.2) but with volume integrals only over the bottom and top boundary layers – that is, the z-integrals are restricted to $h^B \leqslant z \leqslant h^B + \delta$ and $h^T - \delta \leqslant z \leqslant h^T$ respectively. Bounding the right-hand terms of (4.10) using (4.13), (4.14) and the y-analogue of (4.14) gives

$$\begin{aligned}|\langle\theta\boldsymbol{u}\cdot(2\boldsymbol{\nabla}\tau - a\hat{\boldsymbol{z}})\rangle| \leqslant \left(\frac{a+2}{2\delta}\right)&([\langle|h_x^B u\theta|\rangle_B + \langle|h_x^T u\theta|\rangle_T] + [\langle|h_y^B v\theta|\rangle_B + \langle|h_y^T v\theta|\rangle_T] \\ &+ [\langle|w\theta|\rangle_B + \langle|w\theta|\rangle_T]).\end{aligned} \tag{4.15}$$

The thinness of the boundary layers can be exploited to show that the above integrals over boundary layers are small. We do this differently for the terms involving w than for those involving u or v. In the bottom boundary layer, the Cauchy–Schwarz inequality and the fact that θ vanishes at the boundary give

$$|\theta(x, y, z, t)| = \left|\int_{h^B}^{z} \mathrm{d}z'\theta_{z'}(x, y, z', t)\right| \leqslant (z - h^B)^{1/2}\left(\int_{h^B}^{h^B+\delta} \mathrm{d}z\theta_z^2\right)^{1/2}, \tag{4.16}$$

and with no-slip boundaries the same estimates hold with u, v or w in place of θ.

The $\langle|w\theta|\rangle_B$ term can be estimated in the same way as when the boundaries are planar (cf. Constantin & Doering 1996), using the pointwise estimate (4.16) and its analogue for w to find

$$\langle|w\theta|\rangle_B \leqslant \frac{\delta^2}{2}\langle w_z^2\rangle_B^{1/2}\langle\theta_z^2\rangle_B^{1/2} \tag{4.17}$$

$$\leqslant \frac{\delta^2}{4}\left[c\delta\langle w_z^2\rangle_B + \frac{1}{c\delta}\langle\theta_z^2\rangle_B\right] \tag{4.18}$$

for all $c > 0$, where the second line follows from Young's inequality. Adding (4.18) to its counterpart holding in the top boundary layer and then extending integrals to the entire volume yields

$$\langle|w\theta|\rangle_B + \langle|w\theta|\rangle_T \leqslant \frac{\delta^2}{4}\left[c\delta\langle w_z^2\rangle + \frac{1}{c\delta}\langle\theta_z^2\rangle\right]. \tag{4.19}$$

We estimate $\langle|h_x^B u\theta|\rangle_B$ differently from the estimate (4.17) on $\langle|w\theta|\rangle_B$. Using the same procedure would require pulling the pointwise maximum of h^B out of the integral, ultimately giving an upper bound on $\mathscr{F}$ that becomes infinite as this maximum becomes infinite, such as in figure 1(*c*). Instead, we remove θ from the

https://doi.org/10.1017/jfm.2016.528 Published online by Cambridge University Press

integral using the pointwise estimate $|\theta| \leqslant 1$ holding at large times. This estimate follows from the extremum principle $0 \leqslant T \leqslant 1$ holding at large times and from $0 \leqslant \tau \leqslant 1$, which we ensure by requiring $a \in (0, 2)$. Therefore,

$$\begin{aligned}
\langle |h_x^B u\theta| \rangle_B &\leqslant \langle |h_x^B u| \rangle_B && (4.20)\\
&\leqslant \langle (h_x^B)^2 \rangle_B^{1/2} \langle u^2 \rangle_B^{1/2} && (4.21)\\
&\leqslant \left(\delta \iint_\Omega \mathrm{d}x\,\mathrm{d}y\, (h_x^B)^2 \right)^{1/2} \left(\frac{\delta^2}{2} \langle u_z^2 \rangle_B \right)^{1/2} && (4.22)\\
&\leqslant \frac{\delta^{3/2}}{2\sqrt{2}} \left[c' \delta^{3/2} \langle u_z^2 \rangle_B + \frac{1}{c' \delta^{3/2}} \iint_\Omega \mathrm{d}x\,\mathrm{d}y\, (h_x^B)^2 \right], && (4.23)
\end{aligned}$$

where the second line follows from the Cauchy–Schwarz inequality, the third from the estimate (4.16) for u and the last from Young's inequality. Adding (4.18) to its counterpart for the top boundary layer gives

$$\langle |h_x^B u\theta| \rangle_B + \langle |h_x^T u\theta| \rangle_T \leqslant \frac{1}{2\sqrt{2}} \left(c' \delta^3 \langle u_z^2 \rangle + \frac{1}{c'} \iint_\Omega \mathrm{d}x\,\mathrm{d}y [(h_x^B)^2 + (h_x^T)^2] \right). \tag{4.24}$$

The above estimate and its counterpart for the y-direction, along with (4.19), can be applied to (4.15) to find

$$\begin{aligned}
|\langle \theta \boldsymbol{u} \cdot (2\boldsymbol{\nabla}\tau - a\hat{\boldsymbol{z}}) \rangle| \leqslant \left(\frac{a+2}{2} \right) \Bigg[& \delta^2 \left\langle \frac{c'}{2\sqrt{2}} (u_z^2 + v_y^2) + \frac{c}{4} w_z^2 \right\rangle \\
& + \frac{1}{4c} \langle \theta_z^2 \rangle + \frac{1}{\delta} \frac{1}{\sqrt{2} c'} \|\boldsymbol{\nabla} h\|^2 A \Bigg], \qquad (4.25)
\end{aligned}$$

where $A = |\Omega|$ is the horizontal area and

$$\|\boldsymbol{\nabla} h\|^2 := \frac{1}{2A} \iint_\Omega \mathrm{d}x\,\mathrm{d}y (|\boldsymbol{\nabla} h^B|^2 + |\boldsymbol{\nabla} h^T|^2) \tag{4.26}$$

is the mean squared gradient of the boundary heights $h^B(x, y)$ and $h^T(x, y)$. To take advantage of the inequality $\langle u_z^2 + v_z^2 + 2w_z^2 \rangle \leqslant \langle |\boldsymbol{\nabla} \boldsymbol{u}|^2 \rangle$ that follows from incompressibility and no-slip boundary conditions (cf. Constantin & Doering 1994, endnote 9), we choose $c' \equiv c/2\sqrt{2}$ and obtain

$$|\langle \theta \boldsymbol{u} \cdot (2\boldsymbol{\nabla}\tau - a\hat{\boldsymbol{z}}) \rangle| \leqslant \left(\frac{a+2}{2} \right) \left[\delta^2 \frac{c}{8} \langle |\boldsymbol{\nabla} \boldsymbol{u}|^2 \rangle + \frac{1}{4c} \langle |\boldsymbol{\nabla}\theta|^2 \rangle + \frac{1}{\delta} \frac{2}{c} \|\boldsymbol{\nabla} h\|^2 A \right], \tag{4.27}$$

where we have also used $\langle \theta_z^2 \rangle \leqslant \langle |\boldsymbol{\nabla}\theta|^2 \rangle$. The above expression is a bound on the sign-indefinite term of $\mathscr{Q}_1$ involving its two sign-definite terms. Application of this estimate to the definition (4.7) of $\mathscr{Q}_1$ gives

$$\begin{aligned}
\mathscr{Q}_1 \leqslant & \left[(1-\gamma) \frac{a}{Ra} - c\,\delta^2 \left(\frac{a+2}{16} \right) \right] \langle |\boldsymbol{\nabla} \boldsymbol{u}|^2 \rangle \\
& + \left[1 - \frac{1}{c} \left(\frac{a+2}{8} \right) \right] \langle |\boldsymbol{\nabla}\theta|^2 \rangle + \frac{1}{\delta} \frac{1}{c} (a+2) \|\boldsymbol{\nabla} h\|^2 A, \qquad (4.28)
\end{aligned}$$

https://doi.org/10.1017/jfm.2016.528 Published online by Cambridge University Press

provided that τ is defined with $a \in (0, 2)$. We choose c and δ to make the above coefficients on $\langle|\boldsymbol{\nabla u}|^2\rangle$ and $\langle|\boldsymbol{\nabla}\theta|^2\rangle$ non-positive, in which case $\mathscr{Q}_1$ is bounded above by the final term, which has no dependence on the unknown fields $\boldsymbol{u}$ or θ. Our eventual upper bound on $\mathscr{F}$ is minimized by choosing the largest possible δ. This is done by choosing c as small as possible while keeping the $\langle|\boldsymbol{\nabla}\theta|^2\rangle$ coefficient non-positive,

$$c = \frac{a+2}{8}, \tag{4.29}$$

and then choosing δ as large as possible while keeping the $\langle|\boldsymbol{\nabla u}|^2\rangle$ coefficient non-positive,

$$\delta = \sqrt{1-\gamma}\left(\frac{8\sqrt{2a}}{a+2}\right) Ra^{-1/2}. \tag{4.30}$$

When Ra is small this formula produces a value of δ that is too large to properly define τ because the boundary layers would overlap, so our main result will apply only for sufficiently large Ra. As discussed at the end of § 4.6, this restriction can be lifted by defining δ differently at small Ra.

With the c and δ chosen above, $\mathscr{Q}_1$ is bounded by the last term of (4.28), which becomes

$$\mathscr{Q}_1 \leqslant \frac{1}{\sqrt{1-\gamma}}\left(\frac{a+2}{\sqrt{2a}}\right) \|\boldsymbol{\nabla} h\|^2 A Ra^{1/2}. \tag{4.31}$$

This bound on $\mathscr{Q}_1$ holds for the τ defined by (4.9) with δ as in (4.30) and any $a \in (0, 2)$ and $\gamma \in (0, 1)$. Thus, we have shown that one of the three terms composing $\mathscr{F}$ in (4.6) is no larger than $O(Ra^{1/2})$. The next two subsections show the same for the other two terms; hence, $\mathscr{F}$ itself is no larger than $O(Ra^{1/2})$. After all three terms have been estimated, particular values of a and γ will be chosen to obtain an explicit prefactor that is as small as possible.

4.4. *Upper bound on* $\mathscr{Q}_2$

In this subsection the quadratic functional $\mathscr{Q}_2[\boldsymbol{u}]$ defined by (4.8) is bounded above by an expression that is smaller than $O(Ra^{1/2})$. We first show that the sign-indefinite term $\langle\tau w\rangle$ is small by exploiting the thinness of the boundary layers of τ. The fact that τ is non-zero outside the boundary layers is not an obstacle because $\langle\tau w\rangle = \langle\widetilde{\tau} w\rangle$, where $\widetilde{\tau} := \tau - [1/2 + (a/2)(z-(1/2))]$ does vanish outside the boundary layers. The equality $\langle\tau w\rangle = \langle\widetilde{\tau} w\rangle$ holds because $\langle gw\rangle = 0$ for any function $g(z)$ when the boundaries are impenetrable. (This follows from the identity $\langle gw\rangle = \langle\boldsymbol{\nabla}\cdot(\boldsymbol{u}G)\rangle$, where $G(z)$ is an antiderivative of $g(z)$, since $\langle\boldsymbol{\nabla}\cdot(\boldsymbol{u}G)\rangle = 0$.)

Because $\widetilde{\tau}$ vanishes outside the boundary layers, $\langle\tau w\rangle$ can be expressed in terms of integrals over the boundary layers as

$$\langle\tau w\rangle = \langle\widetilde{\tau} w\rangle_B + \langle\widetilde{\tau} w\rangle_T. \tag{4.32}$$

Use of the pointwise bound (4.16) on w in the bottom boundary layer gives

$$|\langle\widetilde{\tau} w\rangle_B| \leqslant \lim_{t\to\infty}\frac{1}{t}\int_0^t \mathrm{d}t' \iint_\Omega \mathrm{d}x\,\mathrm{d}y \left(\int_{h^B}^{h^B+\delta} \mathrm{d}z\, w_z^2\right)^{1/2} \left|\int_{h^B}^{h^B+\delta} \mathrm{d}z (z-h^B)^{1/2}\,\widetilde{\tau}\right| \tag{4.33}$$

$$\leqslant \left(\frac{a+2}{15}\right)\delta^{3/2} \lim_{t\to\infty}\frac{1}{t}\int_0^t \mathrm{d}t' \iint_\Omega \mathrm{d}x\,\mathrm{d}y \left(\int_{h^B}^{h^B+\delta} \mathrm{d}z\, w_z^2\right)^{1/2} \tag{4.34}$$

https://doi.org/10.1017/jfm.2016.528 Published online by Cambridge University Press

$$\leqslant \left(\frac{a+2}{15}\right)\delta^{3/2}A^{1/2}\langle w_z^2\rangle_B^{1/2} \tag{4.35}$$

$$\leqslant \frac{4\gamma}{Ra}\langle w_z^2\rangle_B + \frac{Ra}{16\gamma}\left(\frac{a+2}{15}\right)^2\delta^3 A. \tag{4.36}$$

The second line above is reached after bounding the z-integral of $(z-h^B)^{1/2}\,\widetilde{\tau}$, the horizontal area A appears in the third line after using the Cauchy–Schwarz inequality and in the final line we have used Young's inequality with the intent of making the first coefficient $4\gamma/Ra$. Application of (4.36) and its counterpart in the top boundary layer to (4.32) gives

$$|\langle \tau w\rangle| \leqslant \frac{4\gamma}{Ra}\langle w_z^2\rangle + \frac{Ra}{8\gamma}\left(\frac{a+2}{15}\right)^2\delta^3 A \tag{4.37}$$

$$\leqslant \frac{\gamma}{Ra}\langle|\boldsymbol{\nabla u}|^2\rangle + \frac{(1-\gamma)^{3/2}}{\gamma}\frac{128\sqrt{2}}{225}\frac{a^{3/2}}{a+2}ARa^{-1/2}, \tag{4.38}$$

where the second line has used the definition (4.30) of δ and the estimate $\langle w_z^2\rangle \leqslant (1/4)\langle|\boldsymbol{\nabla u}|^2\rangle$ that follows from incompressibility and no-slip boundary conditions (cf. (5.16) of Constantin & Doering 1996). The functional $\mathscr{Q}_2[\boldsymbol{u}]$ defined by (4.8) is thus bounded by

$$\mathscr{Q}_2 \leqslant \frac{1}{\gamma}\frac{128\sqrt{2}}{225}\frac{a^{5/2}}{a+2}A\,Ra^{-1/2}. \tag{4.39}$$

For convenience, we have used $(1-\gamma)^{3/2}\leqslant 1$ since this does not worsen the leading prefactor of our eventual bound on $\mathscr{F}$. In the next subsection an expression is chosen for γ that is $O(Ra^{-1/2})$. This makes the above estimate $O(1)$ in Ra, so $\mathscr{Q}_2$ makes only a higher-order contribution to our $O(Ra^{1/2})$ bound on $\mathscr{F}$.

4.5. *Upper bound on* $\langle|\boldsymbol{\nabla}\tau|^2\rangle$

In this subsection we bound $\langle|\boldsymbol{\nabla}\tau|^2\rangle$, having already bounded the other two terms composing $\mathscr{F}$ in (4.6). If a particular geometry is of interest one can evaluate $\langle|\boldsymbol{\nabla}\tau|^2\rangle$ exactly and then tune a to minimize the resulting bound on $\mathscr{F}$. This idea is revisited in § 4.7, but first we take the more general approach of bounding $\langle|\boldsymbol{\nabla}\tau|^2\rangle$ above in terms of $\boldsymbol{\nabla}h^T$ and $\boldsymbol{\nabla}h^B$. In this way we establish for all admissible geometries that $\langle|\boldsymbol{\nabla}\tau|^2\rangle$ is no larger than $O(Ra^{1/2})$.

The horizontal derivative τ_x vanishes outside the boundary layers and is bounded by (4.12) in the top boundary layer, and analogously in the bottom one, so its square integral is bounded by

$$\langle\tau_x^2\rangle \leqslant \frac{1}{\delta}\frac{(a+2)^2}{16}\iint_\Omega \mathrm{d}x\,\mathrm{d}y[(h_x^B)^2+(h_x^T)^2]. \tag{4.40}$$

The vertical derivative τ_z is $a/2$ in the interior and is bounded by $(a+2)/4\delta$ in both boundary layers, so

$$\langle\tau_z^2\rangle \leqslant \frac{1}{\delta^2}\frac{(a+2)^2}{16}V_{BL} + \frac{a^2}{4}(V-V_{BL}) \tag{4.41}$$

$$\leqslant \frac{1}{\delta}\frac{(a+2)^2}{8}A + \frac{a^2}{4}V, \tag{4.42}$$

https://doi.org/10.1017/jfm.2016.528 Published online by Cambridge University Press

where V is the volume of the domain, $A = |\Omega|$ is its cross-sectional area and $V_{BL} = 2A\delta$ is the combined volume of the boundary layers. Use of (4.42) along with (4.40) and its analogue for $\langle \tau_y^2 \rangle$ gives

$$\langle |\nabla \tau|^2 \rangle \leqslant \frac{1}{\delta} \frac{(a+2)^2}{8} (1 + \|\nabla h\|^2) A + \frac{a^2}{4} V, \tag{4.43}$$

where the mean squared boundary gradient $\|\nabla h\|^2$ is as defined by (4.26). For the δ we defined by (4.30) when showing $\mathscr{D}_1 \lesssim O(Ra^{1/2})$, the above expression becomes

$$\langle |\nabla \tau|^2 \rangle \leqslant \frac{1}{\sqrt{1-\gamma}} \frac{(a+2)^3}{64\sqrt{2a}} (1 + \|\nabla h\|^2) A\, Ra^{1/2} + \frac{a^2}{4} V \tag{4.44}$$

for all $a > 0$ and $\gamma \in (0, 1)$.

4.6. *Main result*

The three terms composing $\mathscr{F}$ in expression (4.6) have now been bounded above by (4.31), (4.39) and (4.44). Combination of these estimates gives

$$\mathscr{F} \leqslant \frac{1}{\sqrt{1-\gamma}} C_1 A\, Ra^{1/2} + \frac{1}{\gamma} C_2 A\, Ra^{-1/2} + \frac{a^2}{4} V \tag{4.45}$$

for all $a \in (0, 2)$ and $\gamma \in (0, 1)$, where

$$C_1 := \frac{(a+2)^3}{64\sqrt{2a}} + \frac{(a+2)^3 + 64(a+2)}{64\sqrt{2a}} \|\nabla h\|^2, \quad C_2 := \frac{128\sqrt{2}}{225} \frac{a^{5/2}}{a+2}. \tag{4.46a,b}$$

The optimal γ that minimizes (4.45) depends on Ra, and at large Ra this optimal value asymptotes to

$$\gamma = \sqrt{\frac{2C_2}{C_1}}\, Ra^{-1/2}. \tag{4.47}$$

With this choice of γ, the bound (4.45) on $\mathscr{F}$ becomes

$$\mathscr{F} \leqslant \frac{1}{\sqrt{1 - \sqrt{2C_2/C_1}\, Ra^{-1/2}}} C_1 A\, Ra^{1/2} + \left[\sqrt{\frac{C_1 C_2}{2}} A + \frac{a^2}{4} V \right] \tag{4.48}$$

for all $a \in (0, 2)$.

Expression (4.48) is our main result. For any domain where the functions defining the top and bottom boundaries have square-integrable gradients, we have proven that the time-averaged heat flux through the layer, $\mathscr{F}$, can grow no faster than $Ra^{1/2}$ at large Ra. The particulars of the geometry enter through the total fluid volume V, the horizontal area A and the mean squared boundary gradients $\|\nabla h\|^2$ defined by (4.26).

The bound (4.48) is really a family of results; each choice of $a \in (0, 2)$ gives an explicit bound on $\mathscr{F}$ that varies with Ra and $\|\nabla h\|^2$. If the aim is to optimize the bound at large Ra, then a should be chosen to minimize C_1 because the leading behaviour of (4.48) is

$$\mathscr{F} \lesssim A[C_1 Ra^{1/2} + O(1)]. \tag{4.49}$$

https://doi.org/10.1017/jfm.2016.528 Published online by Cambridge University Press

The value of a that minimizes C_1 depends on the boundary geometry since the definition (4.46) of C_1 involves $\|\nabla h\|^2$. If a particular geometry is of interest, one can calculate $\|\nabla h\|^2$ and then choose some $a \in (0, 2)$. To give a concrete bound here we simply fix $a = 2/5$, so

$$C_1 = \frac{27}{50\sqrt{5}} + \frac{327}{50\sqrt{5}}\|\nabla h\|^2 \approx 0.242 + 2.925\|\nabla h\|^2, \tag{4.50}$$

$$C_2 = \frac{256}{3375\sqrt{5}} \approx 0.0340. \tag{4.51}$$

This choice of a minimizes C_1 when the boundaries are planar ($\|\nabla h\|^2 = 0$), and even in the worst case where $\|\nabla h\|^2 \gg 1$ it gives a value for C_1 that is only 22 % larger than optimal. Application of the above C_1 to (4.48) gives an explicit bound on $\mathscr{F}$ whose leading behaviour is

$$\mathscr{F} \lesssim A\left[\left(\frac{27}{50\sqrt{5}} + \frac{327}{50\sqrt{5}}\|\nabla h\|^2\right) Ra^{1/2} + O(1)\right]. \tag{4.52}$$

With planar boundaries the leading prefactor reduces to 0.242, which is unsurprisingly larger than the best known prefactor of 0.027 proven specifically for planar boundaries by Plasting & Kerswell (2003), although not very much larger than the prefactor of 0.167 found by Constantin & Doering (1996).

The bound (4.48) holds only for sufficiently large Ra because our analysis has required that $\gamma < 1$ and that the boundary layers of τ fit in the domain, which happens if $2\delta \leqslant \Delta_h := \min_{x,y}(h^T - h^B)$. For the explicit bound (4.52) obtained by fixing $a = 2/5$, these conditions hold if

$$Ra > \max\left\{\frac{1024}{3645}, \frac{320}{9}\frac{1}{\Delta_h^2}\right\}. \tag{4.53}$$

With planar boundaries this becomes $Ra > 320/9 \approx 35.6$, which is an irrelevant restriction since convection cannot persist if $Ra < 1707.7$. With non-planar boundaries, the occurrence of convection for all $Ra > 0$ means that bounds on $\mathscr{F}$ may be wanted at small Ra. The restriction (4.53) on Ra arose only because we chose δ and γ to be optimal at large Ra, and it is straightforward to modify our analysis to prove a bound holding for all $Ra > 0$. When Ra is too small for (4.47) to obey $\gamma < 1$ one can instead fix a constant value of γ, and when Ra is too small for boundary layers defined by (4.30) to obey $2\delta \leqslant \Delta_h$ one can instead take $2\delta = \Delta_h$.

4.7. *Sinusoidal boundaries*

Consider the example of sinusoidal boundaries, a domain recently simulated in two dimensions by Toppaladoddi *et al.* (2015). Suppose that the top and bottom boundaries are uniform in y and sinusoidal in x with amplitude β and wavelength λ. Let the span in the x-direction be a multiple of λ, so that an integer number of wavelengths fit in the domain. The flow may be either horizontally periodic or bounded by vertical sidewalls. The boundary gradients h_x^B and h_x^T equal $(2\pi\beta/\lambda)\sin(2\pi x/\lambda)$ or translations thereof, so the mean squared boundary gradient is $\|\nabla h\|^2 = 2\pi^2\beta^2/\lambda^2$. Expression (4.52) for the leading behaviour of the bound then becomes

$$\mathscr{F} \lesssim A\left[\left(\frac{27}{50\sqrt{5}} + \frac{327\pi^2}{25\sqrt{5}}\frac{\beta^2}{\lambda^2}\right) Ra^{1/2} + O(1)\right]. \tag{4.54}$$

https://doi.org/10.1017/jfm.2016.528 Published online by Cambridge University Press

It is similarly easy to evaluate (4.52) for other geometries, but we can improve upon this general result by specializing the analysis at an earlier stage.

To illustrate how to improve upon our main result for a particular geometry of interest, let us consider sinusoidal boundaries whose wavelength is twice their amplitude, meaning $\lambda = 2\beta$ and so $\|\nabla h\|^2 = \pi^2/2$. The bound (4.54) then has a leading prefactor of approximately 14.67. This bound exceeds the heat flux in the computations of Toppaladoddi *et al.* (2015) by two orders of magnitude, suggesting much room for improvement. The prefactor of 14.67 is simply the coefficient C_1 defined by (4.46), after we have chosen $a = 2/5$ and used the value of $\|\nabla h\|^2$, but the choice $a = 2/5$ is suboptimal when $\|\nabla h\|^2$ is not small. A simple way to lower the prefactor is to choose $a \approx 1.2124$, which minimizes C_1 when $\|\nabla h\|^2 = \pi^2/2$. This lowers the leading prefactor to approximately 12.15, but we can do still better by revisiting the analysis that led to the expression for C_1.

The leading prefactor of our main result (4.48) is the sum of the leading coefficients of the bound (4.31) on $\mathscr{Q}_1$ and the bound (4.44) on $\langle|\nabla\tau|^2\rangle$. One way to tighten the result is to evaluate $\langle|\nabla\tau|^2\rangle$ exactly instead of bounding it above. Doing so in the case of sinusoidal boundaries with $\lambda = 2\beta$ gives a bound on $\mathscr{F}$ with a lengthy leading prefactor that depends on β and a. For each value of β one can choose the value of a that minimizes the prefactor. Doing so recovers the prefactor of 12.15 when $\beta \ll 1$ but gives a better result as β increases. When $\beta = 0.2$, for instance, the optimal choice $a \approx 1.431$ gives a bound on $\mathscr{F}$ with a leading prefactor of approximately 11.56.

A final way to tighten our main result in some cases is to revisit the bound on $\mathscr{Q}_1$, where the term $\langle|2\tau_x u\theta|\rangle$ was estimated by (4.23). In deriving this estimate, the pointwise bound $|\theta| \leqslant 1$ was used to remove θ from the integral. One could instead remove the pointwise maxima of h_x^B and h_x^T from the integral and then estimate $\langle|u\theta|\rangle$ in the boundary layer in the same way that $\langle|w\theta|\rangle$ was estimated by (4.18). Carrying through this analysis gives an $O(Ra^{1/2})$ upper bound on $\mathscr{F}$ with a leading prefactor that involves not only the mean squared values of $|\nabla h^B|$ and $|\nabla h^T|$ but also their pointwise maxima. Such a result is generally weaker than our main result (4.48) since it requires boundary gradients to be uniformly bounded, but it gives smaller prefactors when the pointwise maxima are fairly small. In the example of sinusoidal boundaries with $\lambda = 2\beta$, this alternate analysis gives leading prefactors that are approximately half as large as in our present analysis.

5. Conclusions

Not unexpectedly, it is more work to bound quantities of physical interest in complicated geometries than in the idealized spatial domains of canonical models. The effort is nonetheless worthwhile since all real geometries are imperfect, and even small-scale wall roughness can significantly alter mean quantities. Here, we have shown how to adapt the background method to establish bounds in complicated geometries. Almost all previous applications of this method have been limited to simple geometries, with the notable exception of Wang (1997). The configuration we have studied is Rayleigh–Bénard convection in a fluid layer whose top and bottom boundary heights are functions of the horizontal position. Our main finding is that the heat transport across the fluid layer, normalized by the temperature difference between the boundaries, is $O(Ra^{1/2})$ at large Ra. This is the same scaling of previously proven bounds for finite-Prandtl-number convection between no-slip planar boundaries. Our bound is consistent with past numerical and laboratory studies of convection between rough boundaries, where growth of the Nusselt number has been either proportional to $Ra^{1/2}$ (Roche *et al.* 2001) or slower.

https://doi.org/10.1017/jfm.2016.528 Published online by Cambridge University Press

A remaining challenge is to remove some of the technical assumptions needed here. Our proof requires the boundary heights to be functions of the horizontal position with square-integrable gradients. This is because we defined the boundary layers of the thermal background field to have a fixed vertical thickness. More general boundary geometries might be tackled by instead defining boundary layers according to their thickness normal to the boundaries. Furthermore, our requirement that side boundaries be planar and vertical might be relaxed with additional effort.

A more ambitious goal for future analysis is to extend the background method to complicated geometries when a background decomposition must be applied to the velocity field, as opposed to a scalar field like the temperature. Such velocity decompositions have been used to prove upper bounds on viscous dissipation in canonical models of shear flows, where simple geometry allows for plane parallel background flows that automatically satisfy incompressibility. In complicated geometries, such as for channel flow between rough walls, the construction of suitable incompressible background flows presents difficulties that are the subject of current research.

Acknowledgements

Much of this research was performed at the Woods Hole Oceanographic Institution's Geophysical Fluid Dynamics Program, substantially supported by US National Science Foundation (NSF) Awards OCE-0824636 and OCE-1332750 and the Office of Naval Research, and at the NSF's Institute for Pure and Applied Mathematics during its 2014 Mathematics of Turbulence program. This work was also supported in part by NSF Awards PHY-1205219 and DMS-1515161, a Simons Fellowship in Theoretical Physics and a John Simon Guggenheim Memorial Foundation Fellowship (C.R.D.). We are furthermore grateful for helpful suggestions from the anonymous referees.

REFERENCES

BUSSE, F. H. 1969 Bounds on the transport of mass and momentum by turbulent flow between parallel plates. *Z. Angew. Math. Phys.* **20**, 1–14.

CHOFFRUT, A., NOBILI, C. & OTTO, F. 2016 Upper bounds on Nusselt number at finite Prandtl number. *J. Differ. Equ.* **260**, 3860–3880.

CILIBERTO, S. & LAROCHE, C. 1999 Random roughness of boundary increases the turbulent convection scaling exponent. *Phys. Rev. Lett.* **82**, 3998–4001.

CONSTANTIN, P. & DOERING, C. R. 1994 Variational bounds on energy dissipation in incompressible flows: shear flow. *Phys. Rev.* E **49**, 4087–4099.

CONSTANTIN, P. & DOERING, C. R. 1995 Variational bounds on energy dissipation in incompressible flows. II: channel flow. *Phys. Rev.* E **51**, 3192–3198.

CONSTANTIN, P. & DOERING, C. R. 1996 Variational bounds on energy dissipation in incompressible flows. III: convection. *Phys. Rev.* E **53**, 5957–5981.

DU, Y.-B. & TONG, P. 1998 Enhanced heat transport in turbulent convection over a rough surface. *Phys. Rev. Lett.* **81**, 987–990.

DU, Y.-B. & TONG, P. 2000 Turbulent thermal convection in a cell with ordered rough boundaries. *J. Fluid Mech.* **407**, 57–84.

GOLUSKIN, D. 2015*a* *Internally Heated Convection and Rayleigh–Bénard Convection*. Springer.

GOLUSKIN, D. 2015*b* Internally heated convection beneath a poor conductor. *J. Fluid Mech.* **771**, 36–56.

HOFFMANN, N. P. & VITANOV, N. K. 1999 Upper bounds on energy dissipation in Couette–Ekman flow. *Phys. Lett.* A **255**, 277–286.

https://doi.org/10.1017/jfm.2016.528 Published online by Cambridge University Press

HOWARD, L. N. 1963 Heat transport by turbulent convection. *J. Fluid Mech.* **17**, 405–432.

HOWARD, L. N. 1972 Bounds on flow quantities. *Annu. Rev. Fluid Mech.* **4**, 473–494.

JEFFREYS, H. 1928 Some cases of instability in fluid motion. *Proc. R. Soc. Lond.* A **118**, 195–208.

JOHNSTON, H. & DOERING, C. R. 2009 Comparison of turbulent thermal convection between conditions of constant temperature and constant flux. *Phys. Rev. Lett.* **102**, 064501.

KERSWELL, R. R. 1997 Variational bounds on shear-driven turbulence and turbulent Boussinesq convection. *Phys.* D **100**, 355–376.

KERSWELL, R. R. 2001 New results in the variational approach to turbulent Boussinesq convection. *Phys. Fluids* **13**, 192–209.

KERSWELL, R. R. 2002 Upper bounds on general dissipation functionals in turbulent shear flows: revisiting the 'efficiency' functional. *J. Fluid Mech.* **461**, 239–275.

LU, L., DOERING, C. R. & BUSSE, F. H. 2004 Bounds on convection driven by internal heating. *J. Math. Phys.* **45**, 2967–2986.

NICODEMUS, R., GROSSMANN, S. & HOLTHAUS, M. 1998 The background flow method. Part 1. Constructive approach to bounds on energy dissipation. *J. Fluid Mech.* **363**, 281–300.

OTERO, J., WITTENBERG, R. W., WORTHING, R. A. & DOERING, C. R. 2002 Bounds on Rayleigh–Bénard convection with an imposed heat flux. *J. Fluid Mech.* **473**, 191–199.

OTTO, F. & SEIS, C. 2011 Rayleigh–Bénard convection: improved bounds on the Nusselt number. *J. Math. Phys.* **52**, 083702.

PLASTING, S. C. & IERLEY, G. R. 2005 Infinite-Prandtl-number convection. Part 1. Conservative bounds. *J. Fluid Mech.* **542**, 343–363.

PLASTING, S. C. & KERSWELL, R. R. 2003 Improved upper bound on the energy dissipation rate in plane Couette flow: the full solution to Busse's problem and the Constantin–Doering–Hopf problem with one-dimensional background field. *J. Fluid Mech.* **477**, 363–379.

LORD RAYLEIGH 1916 On convection currents in a horizontal layer of fluid, when the higher temperature is on the under side. *Phil. Mag.* **32** (192), 529–546.

ROCHE, P. E., CASTAING, B., CHABAUD, B. & HÉBRAL, B. 2001 Observation of the 1/2 power law in Rayleigh–Bénard convection. *Phys. Rev.* E **63**, 045303.

SALORT, J., LIOT, O., RUSAOUEN, E., SEYCHELLES, F., TISSERAND, J.-C., CREYSSELS, M., CASTAING, B. & CHILLÀ, F. 2014 Thermal boundary layer near roughnesses in turbulent Rayleigh–Bénard convection: flow structure and multistability. *Phys. Fluids* **26**, 015112.

SEIS, C. 2015 Scaling bounds on dissipation in turbulent flows. *J. Fluid Mech.* **777**, 591–603.

STRINGANO, G., PASCAZIO, G. & VERZICCO, R. 2006 Turbulent thermal convection over grooved plates. *J. Fluid Mech.* **557**, 307–336.

TOPPALADODDI, S., SUCCI, S. & WETTLAUFER, J. S. 2015 Tailoring boundary geometry to optimize heat transport in turbulent convection. *Europhys. Lett.* **111**, 44005.

VILLERMAUX, E. 1998 Transfer at rough sheared interfaces. *Phys. Rev. Lett.* **81**, 4859–4862.

WAGNER, S. & SHISHKINA, O. 2015 Heat flux enhancement by regular surface roughness in turbulent thermal convection. *J. Fluid Mech.* **763**, 109–135.

WANG, X. M. 1997 Time averaged energy dissipation rate for shear driven flows in $\mathbb{R}^n$. *Phys.* D **99**, 555–563.

WANG, X. M. & WHITEHEAD, J. P. 2013 A bound on the vertical transport of heat in the 'ultimate state' of slippery convection at large Prandtl numbers. *J. Fluid Mech.* **729**, 103–122.

WEI, P., CHAN, T.-S., NI, R., ZHAO, X.-Z. & XIA, K.-Q. 2014 Heat transport properties of plates with smooth and rough surfaces in turbulent thermal convection. *J. Fluid Mech.* **740**, 28–46.

WEN, B., CHINI, G. P., DIANATI, N. & DOERING, C. R. 2013 Computational approaches to aspect-ratio-dependent upper bounds and heat flux in porous medium convection. *Phys. Lett.* A **377**, 2931–2938.

WHITEHEAD, J. P. & DOERING, C. R. 2011*a* Internal heating driven convection at infinite Prandtl number. *J. Math. Phys.* **52**, 093101.

WHITEHEAD, J. P. & DOERING, C. R. 2011*b* Ultimate state of two-dimensional Rayleigh–Bénard convection between free-slip fixed-temperature boundaries. *Phys. Rev. Lett.* **106**, 244501.

WHITEHEAD, J. P. & DOERING, C. R. 2012 Rigid bounds on heat transport by a fluid between slippery boundaries. *J. Fluid Mech.* **707**, 241–259.

https://doi.org/10.1017/jfm.2016.528 Published online by Cambridge University Press

WHITEHEAD, J. P. & WITTENBERG, R. W. 2014 A rigorous bound on the vertical transport of heat in Rayleigh–Bénard convection at infinite Prandtl number with mixed thermal boundary conditions. *J. Math. Phys.* **55**, 093104.

WITTENBERG, R. W. 2010 Bounds on Rayleigh–Bénard convection with imperfectly conducting plates. *J. Fluid Mech.* **665**, 158–198.

https://doi.org/10.1017/jfm.2016.528 Published online by Cambridge University Press